Quantitative Contrasts in the Copolymerization of Acrylate- and Methacrylate-Based Comonomers

Alina M. Alb,[†] Pascal Enohnyaket,[†] Michael F. Drenski,[†] Raja Shunmugam,[‡] Gregory N. Tew,[‡] and Wayne F. Reed*,[†]

Tulane University, Department of Physics, New Orleans, Louisiana 70118, and Department of Polymer Science and Engineering, University of Massachusetts, Amherst, Massachusetts

Received July 25, 2006; Revised Manuscript Received August 31, 2006

ABSTRACT: Automatic continuous online monitoring of polymerization reactions (ACOMP) was used to assess quantitatively the reactivity, average composition drift and distributions, as well as molar mass and intrinsic viscosity evolution of comonomers from the acrylate and methacrylate families during free radical copolymerization. In the latter case, *N*-methacryloxysuccinimide (MASI) was of chief interest because of its promise as a starting material from which highly tailored polymers can be produced by postpolymerization modifications. It was found that the reactivity ratios of MASI with an acrylate, such as butyl acrylate (BA), were widely separated and comparable to the case of methyl methacrylate (MMA) and BA. In contrast, reactivity ratios for MMA/MASI were closer together, consistent with general trends in the literature for MMA copolymerization with other methacrylates. While this is intuitively reasonable from a chemical point of view, this comprehensive online characterization confirms that at least some predictions about MASI copolymerization behavior can be made using the much wider knowledge base for MMA. The disparity between BA/MASI copolymerization compared to MMA/MASI is also seen in the unusual increase in weight-average molar mass and intrinsic viscosity as conversion increases. This work establishes the precedents and methodologies that can be used as a general tool in MASI-based developments and paves the way toward monitoring ATRP copolymerization of MASI, as well as postpolymerization modifications such as hydrolysis and derivitization.

Introduction

Tailoring polymer properties for increased functionality is tremendously important to all areas of contemporary polymer science.[1−3] The polymerization of active ester monomers for postpolymerization modification is attracting increased attention.[4−7] These active ester polymers appear to be excellent candidates for generating a host of novel polymers with applications from biology to electronic materials.[5,8−14] The use of active esters for bioconjugation has been studied for many years, including the attachment of peptides for polymer therapeutics.[5] More recently, the use of these monomers has been extended to more traditional polymer areas.[9−12]

For example, the copolymerization of *N*-acryloxysuccinimide (NASI) and *N*-isopropylacylamide allowed for various hydrophobic functionalities to be incorporated into the polymer backbone while the molecular weight, polydispersity, and primary sequence were held constant.[10] This enabled the impact of these hydrophobic groups on the lower critical solution temperature (LCST) to be decoupled from other molecular parameters such as polydispersity and batch-to-batch compositional differences. Well-defined comblike copolymers with NASI and *n*-butyl methacrylate (BMA) have also been reported.[15] Despite the interest in these active ester monomers, little fundamental data on their reaction kinetics are available. The recent study by Gilbert reported reactivity ratios between NASI and BMA ($r_{NASI} = 0.22$, $r_{BMA} = 0.24$) to ensure that the branch points were distributed randomly along the chain.[13] Pichot and co-workers have reported reactivity ratios of NASI with *N*,*N*-dimethylacrylamide and *N*-acryloylmorpholine ($r_{NASI} = 0.6$, $r_{DMA} = 0.36$; $r_{NASI} = 0.63$, $r_{NMA} = 0.75$).[4,7] In contrast to NASI, even less is known about the reaction kinetics of *N*-methacryloxysuccinimide (MASI).

MASI was chosen to avoid the major byproduct commonly found in the synthesis of NASI[16] and because this monomer is more hydrolytically stable than other common active esters.[17] At the same time, with no previous knowledge of the reactivity ratios with methacrylate monomers, it seemed most reasonable to select MASI over NASI for copolymerization with other methacrylates. The usefulness of MASI was demonstrated by the copolymerization with various monomers, including methyl, *n*-butyl, and poly(ethylene glycol) methyl ether methacrylate. The active esters within these polymers were then quantitatively reacted with a primary amine to create metal−ligand polymers for studies in supramolecular polymer chemistry.[11,12,18] Although copolymers were generated, many questions remained about the reaction kinetics of these monomers. Understanding the fundamental reaction kinetics of these active ester monomers will increase the ability to design new materials and novel molecular architectures. In this report, the polymerization kinetics of MASI with MMA and BA are reported, including the average composition drift and distribution, reactivity ratios, evolution of the copolymer molar mass, and intrinsic viscosity via automatic continuous online monitoring of polymerization reactions (ACOMP).

ACOMP Overview. Automatic continuous online monitoring of polymerization reactions (ACOMP) was introduced in 1998.[19] It is a nonchromatographic technique that requires the continuous withdrawal of a small sample stream from the reactor, which is diluted to the degree that measurements made on the flowing sample are dominated by single particle properties, not by polymer interactions. Typically, combining multiangle light scattering, ultraviolet absorption, viscometry, and differential refractometry allows the determination of monomer conversion and measures of polymer molecular mass. It has been success-

* Corresponding author. E-mail: wreed@tulane.edu.
[†] Tulane University.
[‡] University of Massachusetts.

10.1021/ma0616864 CCC: $33.50
Published on Web 11/02/2006

Scheme 1

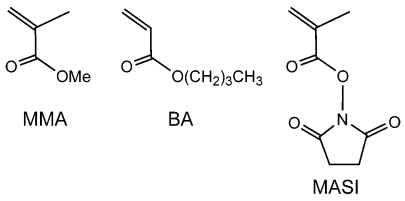

fully applied to many homogeneous polymerization systems: free radical,[20] nitroxide-mediated controlled radical polymerization (CRP),[21] atom transfer radical polymerization (ATRP),[22] step-growth reactions,[23] simultaneous determination of average composition and mass distributions in free radical copolymerization[24] for continuous reactors,[25] and inverse emulsion polymerization.[26] Although no chromatographic columns are used, nonchromatographic means for obtaining average mass distributions and indices of polydispersity were developed and have been presented.[27]

This work makes use of a recent advance in ACOMP, in which a full-spectrum, flow-cell-equipped, UV/visible spectrophotometer is used to simultaneously monitor the conversion of comonomers.[28] This method obtains normalized extinction coefficient basis spectra for each comonomer and uses an analytical error minimization procedure to extract each comonomer concentration each time a full spectrum is read, typically every two seconds. No modeling, peak fitting, or assumptions about spectral structure are required in this approach. The UV spectrum from the highly dilute ACOMP sample at each instant is treated as a linear superposition of the comonomer and copolymer extinction coefficient spectra. The operating hypothesis of this approach is that the comonomer concentrations can be accurately computed, even with low spectral contrast between comonomers at each wavelength, if many wavelengths are used. This hypothesis is born out in the results below.

Materials and Methods

Monomer Synthesis. A 1 L round-bottom flask was charged with the specified amount of *N*-hydroxysuccinimide (25 g, 217.22 mmol) and triethylamine (36.37 g, 260.67 mmol) in 375 mL dichloromethane (DCM). The flask was placed in an ice bath at 0 °C, followed by the dropwise addition of methylmethacryloyl chloride (MAC) (23.3 mL, 238.4 mmol) via an additional funnel. The reaction was stirred for 3 h at RT, then concentrated under reduced pressure, and the excess MAC was removed by dissolving in DCM and washing with DI water, followed by saturated sodium bicarbonate, and finally, with water. The pure organic layer was dried over magnesium sulfate, filtered, and evaporated to a solid. The pure monomer was recovered by recrystallization using ethyl acetate−hexane mixture. Yield: 91%. ^{1}H NMR ($CDCl_3$, ppm): 6.4 (s, H, H_2C═C), 5.9 (s, H, H_2C═C), 2.87 (s, 4H, OSu H), 2.06 (s, 3H, CH_3). Melting point: 100.9 °C. Anal. Calcd $C_8H_9O_4N$: C, 52.45; H, 4.95; N, 7.49. Found: C, 52.27; H, 5.05; N, 7.52.

The other monomers used in this work (MMA and BA) and the initiator, 2,2′-azobis(2-methylpropionitrile) (AIBN) were used as received from Aldrich.

The structures of MMA, BA, and MASI are shown in Scheme 1.

ACOMP System. *N*,*N*-Dimethylformamide (DMF) was used as the ACOMP diluent. The ACOMP system withdrew reactor liquid at 0.1 mL/min, with a total detector flow rate of 2.0 mL/min (i.e. 20/1 dilution), yielding 0.014 g/mL of total monomer in the detector train. The delay time between the reactor and the detector train under that condition was about 150 s. A simple two-pump front end with high-pressure mixing was used in the configuration first introduced by Chauvin et al.[29] A Shimadzu HPLC pump and a Kratos HPLC pump were used in tandem. The concentration of comonomers was kept correspondingly low (30% by mass in DMF) in the reactor to avoid the problems of high viscosity that can be overcome with the full five-pump, dual-mixing chamber instrumentation later introduced by Mignard et al.[30]

The ACOMP detectors included a Shimadzu PDA-20 photodiode array for full-spectrum UV absorbance, a Brookhaven Instruments Corporation BI-MwA 7 angle light scattering instrument, a home-built single capillary viscometer,[31] a dual wavelength Shimadzu UV spectrophotometer (as a redundant cross-check on the PDA-20), and a Waters 410 RI.

ACOMP Procedure. Typically, each experiment started with a solvent (DMF) baseline, followed by the MMA (or BA) baseline, with the monomer solution prepared in a separate reservoir. Meanwhile, the MASI solution was prepared, filtered with 0.45 μm PTFE filter, and mixed with the other comonomer to give the reactor solution. After the first monomer baseline was collected, the line from the reactor pump was switched into the three-neck reactor, where the comonomer solution was prepared and purged with N_2, and the comonomer baseline was taken. Next, the solution was heated to desired temperature (75 °C), and as soon as this was reached, AIBN was added and the reaction began. Aliquots were withdrawn during the reaction for cross-checks using GPC measurements. Different parameters for the MMA/MASI reactions are given in Table 1 and those for BA/MASI in Table 2. Other properties of the monomers and solvent are given in Table 3. Concentration values given are those in the reactor, those in the detector are 5% of these latter. The d*n*/d*c* values for the monomers and their corresponding polymers are given in Table 4.

Multidetector Gel Permeation Chromatography (GPC). GPC work was carried out using the ACOMP detector train, to which two PLgel individual pore size 5 μm and 50 μm chromatographic columns connected in series and an injector with a 0.1 mL loop were added. The elution solvent, DMF, was passed through detectors and columns at 1 mL/min.

By separating monomer from polymer, GPC on discrete, manually withdrawn reaction aliquots, or on samples from the waste stream, allowed a cross-check on the continuous ACOMP conversion and molecular mass data.

Results

Raw Data. Figure 1 shows a typical set of raw data for the free radical copolymerization of MMA and MASI (1A in Table 1). In this case, the monomer concentration was 68/32 based on moles for MMA/MASI. The first 500 s show the DMF baseline, after which MASI was added, and its concentration in the detector train was 0.00488 g/cm^3. The large increase in the RI signal shows the strong positive d*n*/d*c* of MASI in DMF (Table 4). An unusual feature of the MASI baseline is the

Table 1. Reaction Conditions for the MMA/MASI Polymerization Reactions[a]

MMA/MASI (M/M)	C_{MMA} (M)	C_{MASI} (M)	α_{MMA} (s^{-1}) × 10^4	α_{MASI} (s^{-1}) × 10^4	r_{MMA}/r_{MASI}	M_w, (g/mol) × 10^4 f = 0.4/0.8	$[\eta]_w$, (cm^3/g) f = 0.4/0.8	R_g[b] (A) f = 0.4/0.8
1A 68/32	1.24	0.590	6.00	5.0	1.20/0.83	2.5/1.7	13.80/11.58	45.10/37.66
1B 50/50	0.86	0.868	4.80	3.6	1.33/0.75	5.9/9.1	10.80/19.55	55.43/78.09
1C 40/60	0.62	0.956	6.67	5.7	1.17/0.85	4.2/2.7	19.00/14.28	59.65/46.80
1D 100/0	2.49		5.90			1.3/1.2	9.84/9.60	32.28/31.20
1E 0/100		0.321		5.2		0.6/NA	6.24/NA	21.63/NA

[a] [Monomer]/[AIBN] = 50 for all the reactions except for 1A and 1C (= 34). [b] From eq 27.

Table 2. Reactions Conditions for the BA/MASI Polymerization Reactions.

BA/MASI (M/M)	C_{BA} (M)	C_{MASI} (M)	α_{BA} (s^{-1}) × 10^4	α_{MASI} (s^{-1}) × 10^4	r_{BA}/r_{MASI}	M_w, (g/mol) × 10^4 $f = 0.4/0.8$	$[\eta]_w$, (cm^3/g) $f = 0.4/0.8$	R_g[b] (A) $f = 0.4/0.8$
2A 92/8	1.62	0.143	14	27	0.515/1.94	3.6/3.9	17.0/20.3	54.55/59.22
2B 74/26	1.26	0.450	9.7	19	0.520/1.93	4.0/5.3	19.0/25.0	58.74/70.57
2C 53/47	0.9	0.804	6.9	13	0.531/1.88	5.8/1.1	20.6/27.5	68.15/91.87
2D 31/69	0.54	1.185	9.3	10	0.911/1.10	13/22	18/NA	85.40/NA
2E 100/0	1.8		22			4.1/3.4	17.36/16.6	57.40/52.90

[a] [Monomer]/[AIBN] = 50 [b] From eq 27.

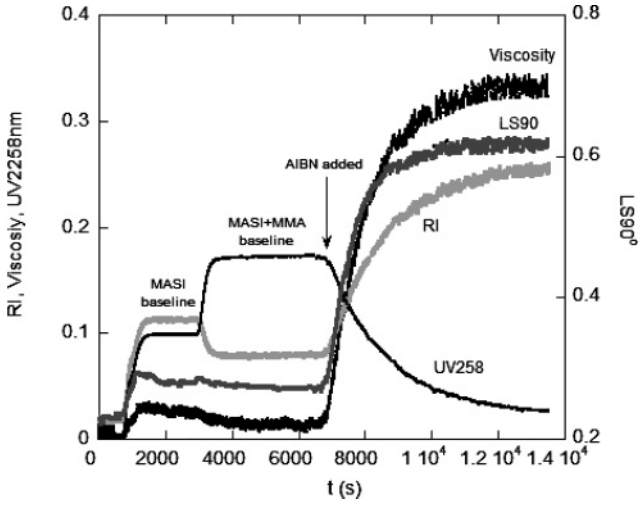

Figure 1. Raw data for reaction 1A in Table 1.

Table 3. Different Parameters for Solvent and Monomers Used in the Polymerization Reactions Presented above

	DMF	MMA	BA
density, ρ (g/cm^3)	0.944	0.936	0.894
refractive index, n	1.43	1.414	1.418

Table 4. dn/dc Values for BA, MMA, MASI, and Their Respective Polymers

	$dn/dc_{monomer}$ (cm^3/g)	$dn/dc_{polymer}$ (cm^3/g)
BA 100%	$-0.0117 \pm 25\%$	0.0410
MMA 100%	$-0.0153 \pm 15\%$	0.0693
MASI 100%	$0.0561 \pm 0.95\%$	0.1150

significant increase in light scattering and viscosity signals for a simple, low-molecular-weight monomer. Such signals indicate the presence of structures whose molar mass is significantly higher than that of the MASI monomer. These are most likely polymers or aggregates of polymers from autopolymerization of MASI despite the use of freshly recrystallized monomer. For LS data analysis, the excess over this baseline was used. GPC measurements on starting reactor aliquots confirm this interpretation as discussed below.

At 3000 s, MMA was added, and its concentration in the detector train was 0.00503 g/cm^3, while MASI maintained its previous concentration. There was no further change in LS, consistent with the small molecule nature of MMA. The decrease in the RI signal is due to the negative value of d*n*/d*c* for MMA in DMF (Table 4).

The reaction was initiated at 7000 s by AIBN, and the three signals for LS (at 90°), viscosity, and RI increase, while the UV258 signal decreases. LS and viscosity increase due to the increasing concentration of polymer in the reactor, and RI increases because d*n*/d*c* of the resulting polymer is larger than the monomeric forms. The full seven-angle LS data indicate that the copolymers produced are well-dispersed chains, not aggregates, because the slopes of Kc/I vs q^2 are nearly zero

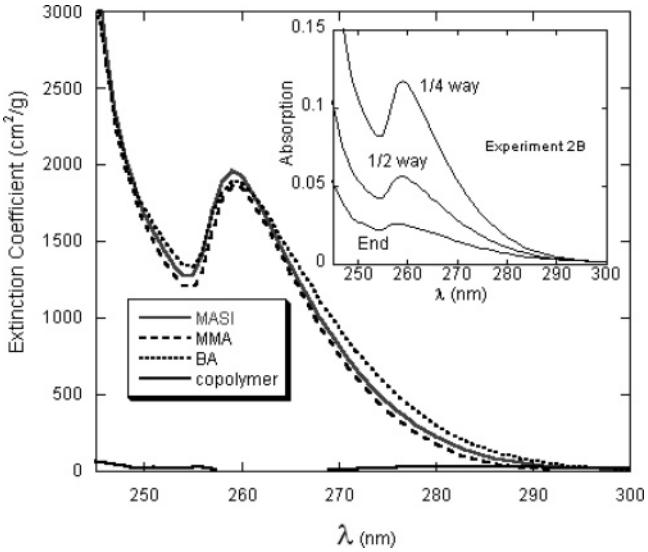

Figure 2. Comonomer and polymer basis extinction coefficient spectra. Each one is averaged over the experiments shown in Tables 1 and 2. The inset shows the evolution of the UV spectra for experiment 2B at time points $^1/_4$ and $^1/_2$ of the way through the reaction and the final spectrum.

throughout the reaction (i.e., radius of gyration below 10 nm). This distinction is important because GPC experiments performed on end-products several days after the ACOMP experiments showed wide-scale aggregation of the MASI-containing chains themselves, which is discussed below. The observed decrease in UV258 intensity confirms monomer consumption as the reaction progresses.

Figure 2 shows the extinction coefficient spectra for MASI, MMA, BA, and a typical copolymer of MASI. The spectra shown are the averages of at least four separate spectra and indicate very little contrast between the three monomers. In fact, attempts to use just two wavelengths while solving two simultaneous equations for the two unknown monomer concentrations at each instant of conversion failed due to the lack of spectral contrast at any pair of wavelengths. Hence, the recently developed approach in ACOMP that uses extended wavelength range spectral analysis was fruitfully applied here.[28] The results below show that this hypothesis is surprisingly well validated even in the current situation of very little spectral contrast.

Concentration Data. The inset to Figure 2 shows a typical evolution of the UV spectra during a reaction (Experiment 2B) at three different periods of the reaction. These types of spectra, taken every 2 s, are used to compute the comonomer concentrations, according to the algorithm mentioned above.

Figure 3a shows the mass concentrations of each comonomer during a MASI/MMA reaction (1A in Table 1), as well as first-order fits to them. The time axis is set so that $t = 0$ is the beginning of the reaction. In this work, each wavelength was equally weighted (statistical weight of unity for each point) in computing the concentrations because the absolute error for each

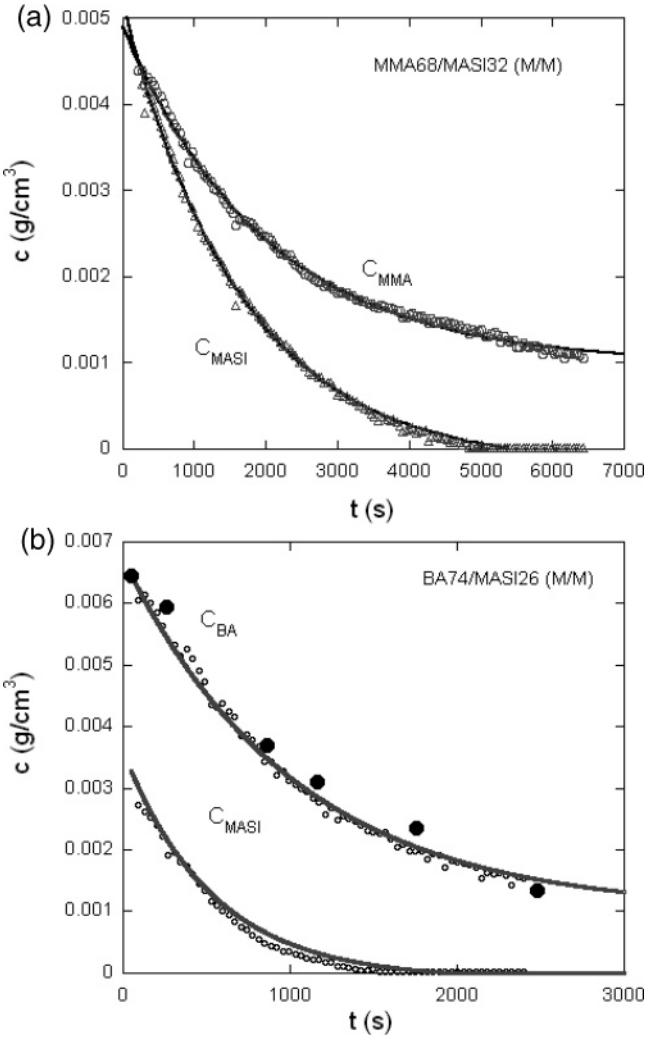

Figure 3. (a) Comonomer concentration data for MMA and MASI obtained from the full spectrum UV approach for experiment 1A from Table 1. (b) Comonomer concentration data for BA and MASI obtained from the full spectrum UV approach for experiment 2B from Table 2. The large solid circles are concentrations of BA obtained from GPC on manually withdrawn aliquots.

wavelength is essentially the same. These data serve as the basis for the subsequent composition drift, average distribution computations, and the determination of the reactivity ratios. Mass concentration of any species A is represented throughout as c_A, whereas the molar concentration is represented as $[A]$.

Figure 3b shows comonomer concentration data for a MASI/BA reaction (2B in Table 2). Exponential fits to each comonomer decay are shown in Figure 3a and b and match the data well. In addition, larger dark circles for the BA concentration in Figure 3b, determined independently by GPC from aliquots manually withdrawn during the reaction, show very good agreement with the concentration obtained from ACOMP. Technical problems with the elution of MASI in GPC did not allow simultaneous determination of MASI concentration.

Reactivity Ratios. It is important to point out that obtaining the comonomer concentrations via ACOMP is model-independent. The average composition, molar mass, and intrinsic viscosity distributions are likewise determined from the detector signals in model-independent fashion. The notion of reactivity ratios, and the various formulations to express them, in contrast, are model-dependent. Computation of sequence lengths that use reactivity ratios are also model-dependent. In some sense, ACOMP makes unnecessary the use of reactivity ratios because

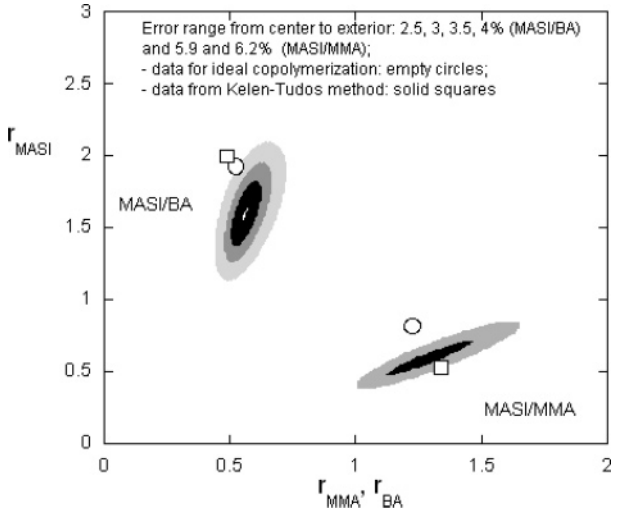

Figure 4. Error plots for r_A and r_B for MASI/MMA and MASI/BA. The different error contour levels are indicated in the figure. Hollow circles are the "ideal" results from eq 7. Hollow squares are Kelen−Tudos results.

it yields the average composition distribution as it evolves during the reaction and automatically detects any unexpected or nonideal effects that may occur in a reaction, but which are not normally predicted by idealized models. Nonetheless, the reactivity ratios are still important for their predictive power, their practical use in helping to optimize reactions, their inherent theoretical interest, and for historical reasons. The value of reactivity ratios obtained by any specific data analysis means, however, are only as meaningful as the idealized model employed in their computation. Many ways of obtaining reactivity ratios from comonomer concentration data have been used, including linearization, full nonlinear approaches, numerical minimization of errors, etc. It is beyond the scope of this work to consider the many historical problems associated with the determination and meaningfulness of reactivity ratios. Rather, a straightforward approach is used below, and the results can be immediately compared with the existing literature.

In the simplest model for propagation in free radical copolymerization, it is assumed that the rate of reaction for a given comonomer depends only on which monomer bears the radical at the chain terminus, and penultimate effects are ignored. For the molar concentrations of monomer $[A]$ and $[B]$, this leads to propagation equations of the form

$$-\frac{d[A]}{dt} = k_{AA}[A][A^*] + k_{BA}[A][B^*] \quad (1a)$$

$$-\frac{d[B]}{dt} = k_{BB}[B][B^*] + k_{AB}[B][A^*] \quad (1b)$$

where A^* and B^* are the propagating radicals of A and B, respectively. The quasi-steady-state approximation assumes that the rate at which $[A^*]$ and $[B^*]$ change is low compared to the other rates in the reaction ($d[A^*]/dt \approx 0$, and similarly for B^*). This is a major constraining assumption in the model. The usual Mayo−Lewis copolymer equation is then

$$\frac{d[A]}{d[B]} = \frac{[A]}{[B]}\left(\frac{r_A[A] + [B]}{[A] + r_B[B]}\right) \quad (2)$$

where the reactivity ratios r_A and r_B are defined as

$$r_A = \frac{k_{AA}}{k_{AB}}, \qquad r_B = \frac{k_{BB}}{k_{BA}} \tag{3}$$

Because the comonomer conversion kinetics are known from ACOMP, eq 2 offers an immediate and simple means of determining r_A and r_B from the initial conversion rates $(d[A]/dt)_{t=0}$ and $(d[B]/dt)_{t=0}$.

$$\frac{(d[A]/dt)_{t=0}}{(d[B]/dt)_{t=0}} = \left(\frac{r_A[A]_0/[B]_0 + 1}{[A]_0/[B]_0 + r_B}\right) \tag{4}$$

Figure 4 shows error contours for the values of r_A and r_B for the MASI/MMA and MASI/BA data using eq 4, and computing the ratio on the left-hand side in three different ways: (i) linear fit to the initial conversion, (ii) rate constant resulting from an exponential fit to early conversion, and (iii) rate constant resulting from an exponential fit to the entire conversion curve, including an adjustable final baseline, to account for the experimental fact that monomer is not always fully consumed at long times. The ratios from each determination are weighted equally in the error computation. The contours were computed by forming a parameter space grid of pairs of discrete values for r_A and r_B and then computing the error in terms of the difference between experimental and theoretical points, divided by the experimental value for each point. The square root of the sum of the squares of this error for all points, divided by the number of points, gives the root-mean-square error, whose contours are depicted in Figure 4. The higher errors for the MASI/MMA determination reflect the fact that there were fewer experiments available and their noise levels were higher than the MASI/BA experiments.

The average values and standard deviations of r_A and r_B for each comonomer pair are given in Table 5, under the heading "combined kinetic results, by eq 4".

It should be emphasized that the comonomer conversion curves in this work are well approximated by exponential fits of the form

$$[A](t) = [A]_0 \, e^{-\alpha_A t} \tag{5a}$$

$$[B](t) = [B]_0 \, e^{-\alpha_B t} \tag{5b}$$

When this is the case, then the Mayo−Lewis equation becomes

$$\frac{\alpha_A}{\alpha_B} = \frac{r_A[A](t) + [B](t)}{[A](t) + r_B[B](t)} \tag{6}$$

It is straightforward to show that, in the case of first-order monomer conversion, the only way this equation can hold is if

$$r_A = \frac{\alpha_A}{\alpha_B}, \qquad r_B = \frac{\alpha_B}{\alpha_A} \tag{7}$$

It is hence also true in this case that $r_A \cdot r_B = 1$. Table 4 lists the averages and standard deviations of r_A and r_B for each pair of monomers obtained from eq 7 and the exponential fits over the whole range of conversion with the adjustable final baseline to account for incomplete monomer consumption. These are given under the heading "ideal".

The instantaneous mole fraction of monomer A, [*A*], incorporated, $F_{A,inst}$, is given by

$$F_{inst,A} \equiv \frac{d[A]}{d[A+B]} = \frac{r_A f_A^{\,2} + f_A(1-f_A)}{r_A f_A^{\,2} + 2f_A(1-f_A) + r_B(1-f_A)^2} \tag{8}$$

where f_A and f_B are the mole fractions of monomer A and B, respectively, at any instant

$$f_A = \frac{[A]}{[A]+[B]}, \qquad f_B = \frac{[B]}{[A]+[B]} \tag{9}$$

$F_{inst,B}$ is obtained by interchanging the subscripts A and B. These expressions form the basis for finding composition as a function of conversion and determining sequence length distributions. Total fractional molar monomer conversion *f*, is given by

$$f = 1 - \frac{[A]+[B]}{[A]_0 + [B]_0} \tag{10}$$

The rates α_A and α_B for the various experiments are given in Tables 1 and 2, and a summary of these averages and standard deviations for reactivity ratios is given in Table 5. The average values for MASI/MMA, $r_{MASI} = 0.69 \pm 0.15$ and $r_{MMA} = 1.32 \pm 0.08$, are more similar to each other than methacrylate/acrylate reactivity ratios as expected due to the fact that they are both methacrylates. For MASI/BA, the average reactivity ratios found (Table 5) are $r_{BA} = 0.53 \pm 0.04$ and $r_{MASI} = 1.89 \pm 0.13$. The ratios for MASI/BA are fairly close to the literature averages for MMA/BA, confirming the initial chemical intuition that the MASI/MMA (methacrylate/methacrylate) pair would have closer reactivity ratios than an MASI/acrylate (methacrylate/acrylate) pair; i.e., it is the nature of the reactive vinyl bond and its immediately adjacent bonded groups that have a greater impact on reactivity than the −O− linked side groups more distant from the vinyl bond.

Values for reactivity ratios obtained from the comonomer conversion rate constants via eqs 4 and 7 were cross-checked with the frequently used Kelen−Tudos method.[32] On the basis of the ACOMP comonomer conversion data, the reactivity ratios obtained by the Kelen−Tudos method were in good agreement with those found via the rate constant approach and are shown in Table 5. Their values are weighted into the average values from all methods used.

Table 5 gives an extensive compilation of reactivity ratios for MMA with other methacrylates, shown as r_{MMA} and r_2, where r_2 is the companion methacrylate comonomer to MMA. The average literature value of $r_{MMA} \cdot r_2 = 0.91 \pm 0.29$; i.e., this product is close to the "ideal" value of unity. The product $r_{MASI} \cdot r_{MMA} = 0.91$ and $r_{MASI} \cdot r_{BA} = 1.00$, from Table 5. Furthermore, if the larger of the ratios r_{MMA}/r_2 and r_2/r_{MMA} is taken, the average is found to be 2.2 ± 1.0. In this work, $r_{MMA}/r_{MASI} = 1.91$, whereas $r_{MASI}/r_{BA} = 3.55$, much larger than the average ratio found for MMA/methacrylate pairs. Similarly, the literature average for $r_{MMA}/r_{BA} = 6.4 \pm 0.50$, again showing the much wider disparity between methacrylate/acrylate pairs. As usual, these conclusions must be tempered by the fact that there is frequently a wide variation in reactivity ratios in the literature, often due to the evaluation technique.[33]

Composition Drift. The comonomer profiles can be used to compute the composition drift of the copolymer chains during synthesis. The average instantaneous molar fraction of MASI by mass in a copolymer chain formed at any given moment is

$$F_{inst,MASI} = \frac{d[MASI]}{d([MASI]+[MMA])} \tag{11}$$

Table 5. Table of Reactivity Ratios

reactivity ratios from this work		
comonomer pair 1/2	r_1	r_2
MASI/MMA, average all methods	0.69 ± 0.15	1.32 ± 0.08 (MMA)
MASI/MMA, ideal	0.81± 0.05	1.23 ± 0.08(MMA)
MASI/MMA, combined kinetic results, by eq 4	0.73 ± 0.12	1.39 ± 0.25 (MMA)
MASI/MMA, Kelen−Tudos	0.52 ± 0.12	1.35 ± 0.08 (MMA)
MASI/BA, average all methods	1.89 ± 0.13	0.53 ± 0.04 (BA)
MASI/BA, ideal	1.92 ± 0.02	0.52± 0.08 (BA)
MASI/BA, combined kinetic results, by eq 4	1.73 ± 0.16	0.58 ± 0.06 (BA)
MASI/BA, Kelen−Tudos	1.99 ± 0.01	0.50 ± 0.01 (BA)
MMA/BA (literature)	2.29 ± 0.40	0.36 ± 0.06
literature values for MMA and other methacrylate comonomers		
comonomer	r_{MMA}	r_2
HEMA[46]	0.62	2.03
PEGMA[45]	0.75	1.33
4-benzyloxycarbonylphenyl methacrylate [47]	0.50	1.50
2-(dimethylamino)ethyl methacrylate[48]	1.07	1.13
4-methylbenzyl methacrylate[49]	0.77	0.97
butyl methacrylate[50]	∼1.0	∼1.0
2-dimethylaminoethyl methacrylate[51]	0.74	1.30
2-diethylaminoethyl methacrylate[45]	0.89	1.27
2-benzylmethylaminoethyl methacrylate[45]	0.59	0.34
(2,6-diphenyl)phenyl methacrylate[52]	1.42	0.48
2-(*N*-phthalimido)ethyl methacrylate[53]	2.08	0.48
(2-phenyl-1,3-dioxolan-4-yl)methyl methacrylate[54]	0.55	1.74

Figure 5a shows the composition drift, expressed as $F_{inst,MASI}$ vs total fractional molar conversion f, for MASI/MMA (M/M) copolymers for selected comonomer ratios. As expected, the higher reactivity ratio of MMA for this comonomer pair means that MMA depletes more quickly than MASI, leading to chains progressively richer in MASI.

Figure 5b shows the composition drift, expressed as $F_{inst,MASI}$ vs total fractional molar conversion, for BA/MASI (M/M) copolymers for selected comonomer ratios. In this case, MASI has the higher reactivity ratio, leading to its earlier depletion and therefore toward chains with less MASI.

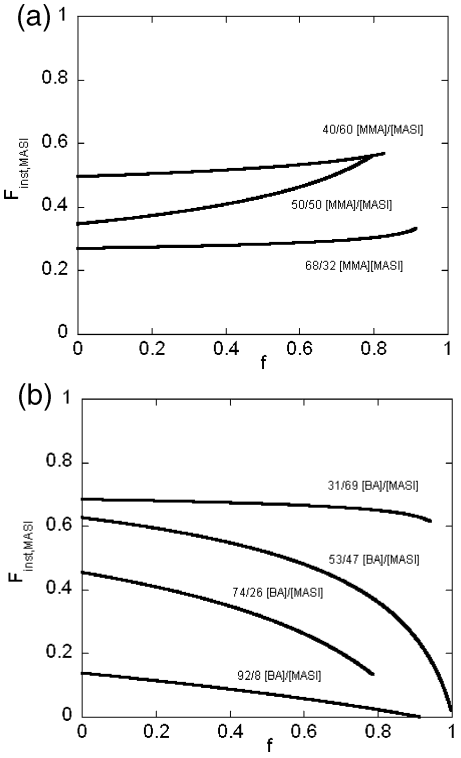

Figure 5. (a) Average composition drift, represented as $F_{inst,MASI}$ vs total molar monomer conversion f for the three MMA/MASI copolymerization experiments in Table 1. (b) Average composition drift, represented as $F_{inst,MASI}$ vs total molar monomer conversion f for the four BA/MASI copolymerization experiments in Table 1.

Average Molar Composition Distribution. The average molar composition distribution can be computed from the above data according to

$$z = \frac{df}{dF_{inst,MASI}} \tag{12}$$

where $zdF_{inst,MASI}$ is the fraction of the total population of chains with molar composition of MASI between $F_{inst,MASI}$ and $F_{inst,MASI} + dF_{inst,MASI}$. The computation of z is shown in Figure 6a for MASI/MMA and in Figure 6b for MASI/BA. As expected, the wider disparity of reactivity ratios between BA and MASI leads to broader, shorter distributions compared to the much narrower, taller distributions for MMA/MASI.

Average Sequence Lengths. While the composition distribution for a copolymer provides important information on compositional heterogeneity, it reveals nothing about the sequence distribution of the copolymers. For example, a copolymer composed of $N/2$ monomers of A and $N/2$ monomers of B could have average sequence distributions ranging all the way from 1, for an alternating copolymer ($r_1 = r_2 = 0$), to $N/2$ for a diblock copolymer ($r_1, r_2 \rightarrow \infty$). The "blockiness" of the copolymer is frequently of paramount importance in determining many types of behavior of the copolymer. In the terminal model for copolymerization, the statistical copolymers produced depend on the conditional probability of adding monomer A to a propagating A^* and B^*, and vice versa.

Let W_{AA} be the probability that the propagating radical of monomer A, A^*, adds to A, that is

$$W_{AA} = \frac{k_{AA}[A][A^*]}{k_{AA}[A][A^*] + k_{AB}[B][A^*]} \tag{13}$$

where k_{AA} and k_{AB} are the rate constants for A and B adding to A^*, respectively. Using the reactivity ratios, this can be expressed, at any total molar monomer conversion point f, during the reaction as

$$W_{AA}(f) = \frac{r_A f_A(f)}{f_A(f)(r_A - 1) + 1} \tag{14}$$

The probability of having a sequence of k monomers in a row of type A, followed by a monomer B, $P_{A,k}$, then follows the well-known geometric distribution[34,35]

$$P_{A,k} = (1 - W_{AA}){W_{AA}}^{k-1} \tag{15}$$

$P_{A,k}(f)$ from ACOMP measurements at each point f is hence the instantaneous sequence length distribution. The moments of this distribution are well-known. The instantaneous number average sequence length of monomer A, $\langle N_A\rangle_n$, at conversion point f, is

$$\langle N_A\rangle_n(f) = \frac{1}{1 - W_{AA}(f)} \tag{16}$$

while the instantaneous weight average sequence length of A, $\langle N_A\rangle_w$ is

$$\langle N_A\rangle_w(f) = \frac{1 + W_{AA}(f)}{1 - W_{AA}(f)} \tag{17}$$

The cumulative values of the number and weight averages,

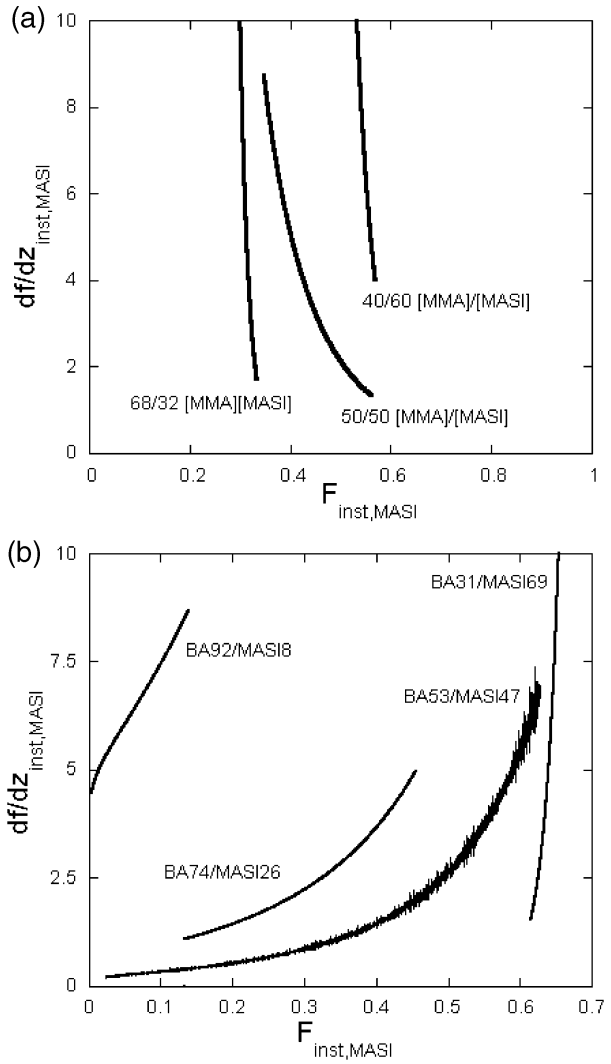

Figure 6. (a) Average composition distribution for the three MMA/MASI experiments in Table 1. (b) Average composition distribution for the four BA/MASI experiments in Table 1.

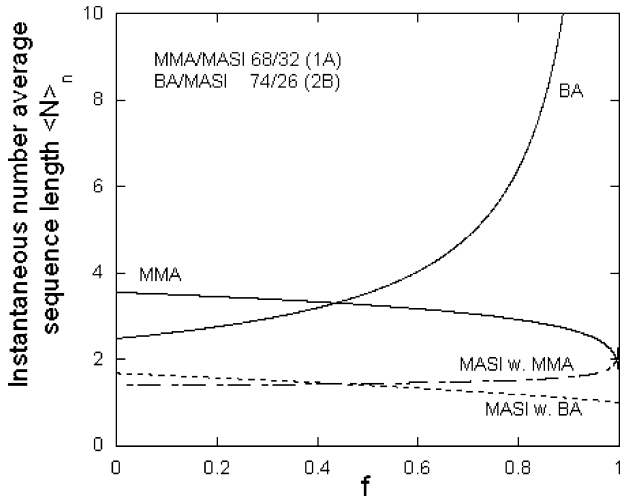

Figure 7. Instantaneous number average sequence lengths for BA/MASI and MMA/MASI of similar starting compositions. The very large increase in sequence length for BA is due to the wide difference in reactivity ratios for BA/MASI.

$\langle N_A\rangle_{n,cumu}$ and $\langle N_A\rangle_{w,cumu}$, can be found by simply summing, or integrating, over all conversion points

$$\langle N_A\rangle_{cumu}(f) = \frac{\int_0^p \langle N_A\rangle(f')\,df'}{f} \tag{18}$$

where the cumulative averages of any moment (e.g., n or w) is obtained by using the corresponding instantaneous average in the integrand.

To obtain the appropriate expressions for monomer B, the subscript B is substituted for A in each variable in the above equations.

Figure 7 shows number-average sequence lengths vs f for MMA/MASI and BA/MASI whose starting molar compositions were similar. MMA/MASI chains maintain similar sequence lengths of MMA throughout conversion, whereas due to the much larger difference in reactivity ratios for BA/MASI, there is a very large increase in BA sequence lengths for chains produced later in conversion because MASI is consumed more rapidly than BA.

Weight-Average Molar Mass M_w and Intrinsic Viscosity $[\eta]_w$. Stockmayer[36] and Benoit and Bushuk[37] detailed the challenges of obtaining M_w for copolymers from light scattering data. For homopolymers, the Zimm[38] single contact approximation is generally used to determine M_w, z-average mean square radius of gyration $\langle S^2\rangle_z$, and the second virial coefficient A_2, via extrapolation to $c_p = 0$ and $q = 0$ of the following expression:

$$\frac{K'\nu^2 c_p}{I(q,c_p)} = \frac{1}{M_w}\left(1 + \frac{q^2\langle S^2\rangle_z}{3}\right) + 2A_2 c_p + O({c_p}^2) \tag{19}$$

where c_p is the concentration of the homopolymer in the detector, q is the scattering vector defined as

$$q = \frac{4\pi n}{\lambda}\sin(\theta/2) \tag{20}$$

and θ is the angular position of the scattering detector. K' is an optical constant. For a vertically polarized light, K is given as

$$K' = \frac{4\pi^2 n^2}{N_A \lambda^4} \tag{21}$$

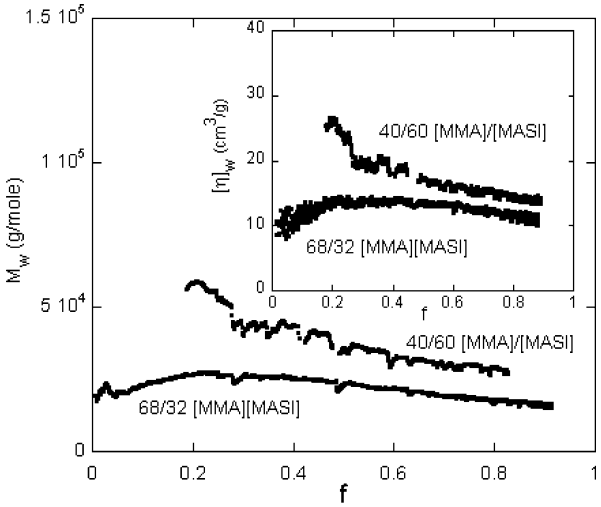

Figure 8. M_w vs conversion for experiments 1A and 1C in Table 1. The inset shows the corresponding $[\eta]_w$ for the same experiments.

and ν is the value of $\partial n/\partial c_p$ measured for the copolymer solution, which is given by

$$\nu = \frac{\partial n}{\partial(c_{pA} + c_{pB})} = y\nu_A + (1 - y)\nu_B \tag{22}$$

and y is the mass fraction of accumulated polymer composed of A

$$y = \frac{c_{pA}}{c_{pA} + c_{pB}} \tag{23}$$

The quantity $K'\nu^2/I(q,c_p)$ extrapolated to $c_p = 0$ for a copolymer, whose $\langle S^2\rangle^{1/2} \ll \lambda$, present in a solution of total copolymer concentration c_p, yields only an apparent molecular weight, M_{ap}:

$$\frac{1}{M_{ap}} = c_p \xrightarrow{\lim} 0 \frac{K'\nu^2 c_p}{I(q,c_p)} \tag{24}$$

To obtain the correct M_w for a copolymer of unknown composition, it was hence traditionally necessary to perform light scattering experiments in three different solvents (i.e., three different values each for ν_A and ν_B) to determine the three unknowns M_w, M_A, and M_B. The introduction of ACOMP and its ability to monitor the evolution of the average composition distribution allows integration of the Stockmayer−Benoit equations so that M_w can be monitored online, as was recently demonstrated.[24] The following results on M_w make use of the procedure developed in ref 24.

Figure 8 shows M_w and $[\eta]_w$ vs f for two of the MMA/MASI reactions. The MMA/MASI M_w and $[\eta]_w$ resemble what is usually obtained for homopolymers because the values either remain constant or decrease in time. This tendency might be expected from the fact that methacrylates normally exhibit this type of behavior and that the reactivity ratios for MASI/MMA are fairly close. As a result, the evolution of M_w and $[\eta]_w$ resembles that of a homopolymer. The decrease of M_w vs conversion is usually taken as evidence that the quasi-steady-state approximation (QSSA) is valid and that the radical concentration varies very slowly in time, if at all.

In contrast, parts a and b of Figure 9 show there is an unusual increase in both M_w and $[\eta]_w$ for the BA/MASI copolymers, and final values of M_w above 10^5 are reached in some cases. Although a definitive explanation is not sought here, the

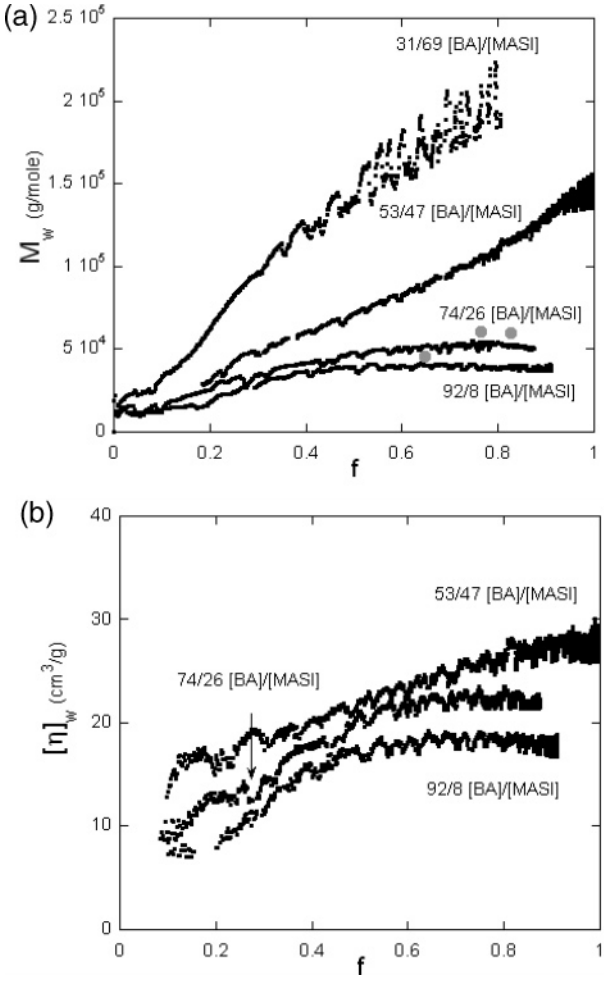

Figure 9. (a) M_w vs conversion for the four BA/MASI experiments in Table 2. (b) $[\eta]_w$ vs conversion for the four BA/MASI experiments in Table 2.

increasing M_w and $[\eta]_w$ may be related to several possible effects: (1) The large disparity in the MASI/BA reactivity ratios (including possible penultimate effects), (2) branching, including that due to radical transfer to polymer, and (3) the poor solubility of MASI-based polymers. The fact that the angular light scattering envelope during ACOMP experiments did not show unusual curvature or slope makes the poor solubility of MASI copolymers unlikely. It has often been found that alkyl acrylates, such as BA, have polymerization rates, $d[BA]/dt$ that are proportional to $[BA]^d$, where d ranges from 1.4 to 1.8, instead of $d = 1$.[38−41] Explanations include chain-length dependence of termination rate coefficients,[42] monomer/solvent complexation,[43] and intrachain radical transfer to form a propagating, midchain radical, leading to a form of branching.[44,45] Presumably, there could be a corresponding interchain end to midchain transfer as well, that could lead to reinitiation and increased M_w of "dead" chains.

It might be added that $d = 1$ is expected only if the decomposition of initiator I_2 is rate controlling in the production of radicalized monomer. Otherwise, if the diffusion controlled encounter of initial radicals I^* with monomer is on the order of decomposition, or itself rate controlling, then $d > 1$.

If $d > 1$ (e.g., $d = 1.4-2$), the monomer decay curves will not be simple first order. However, solving for $[M](t)$ under these scenarios leads to curves that will behave very much like first-order curves when experimental noise is included. The kinetic chain length Λ is given by the ratio of the probability of propagation to termination, where possible transfer is ignored

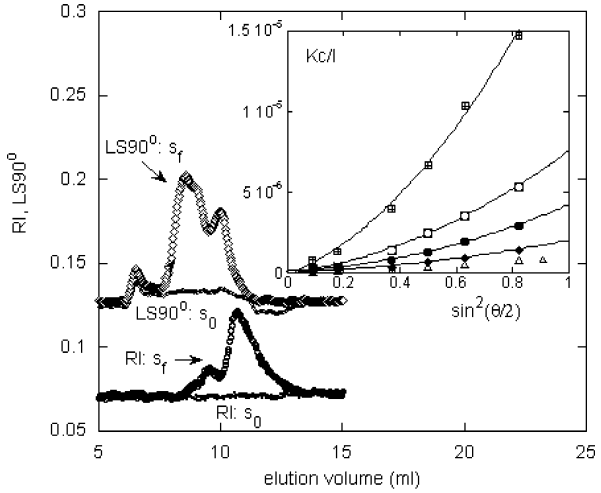

Figure 10. Raw GPC data for aliquots withdrawn for BA/MASI experiment 2B in Table 2 before and at the end of the reaction.

here. Factoring the Mayo−Lewis equation and rearranging yields

$$\Lambda = \frac{A^* k_{12}(r_1 A + 2B + r_2 B^2/A)}{k_{t11}A^{*2} + k_{t12}A^*B^* + k_{t22}B^{*2}} \tag{25}$$

A and B, and A^* and B^*, are the molar concentrations of monomers A and B, and radical A and B, respectively, and the rate constants in the denominator are the termination rate constants for pairs of radicals. A^* and B^* depend on both the initiator decomposition rate and whether the production of each is rate limited by radical decomposition or diffusion controlled encounters of A and B with I^*. If A^* and B^* are each approximately constant, as per the QSSA, then Λ cannot possibly increase, absent branching. The data, however, give incontrovertible proof that M_w and $[\eta]_w$ increase.

While branching may occur, (1) is also possible, if $A^* = a\mathrm{A}$ and $B^* = b\mathrm{B}$, where a and b are constants; i.e., initiation of monomers is rate limiting compared to initiator decomposition. If this expression is used, and a/b are obtained from the inverse ratio of the masses for the homopolymers shown in Tables 1 and 2, r_1 and r_2 are taken from Table 5, and all the termination rates are set equal as a first approximation, it is indeed found that for MASI/MMA, N_w will decrease with conversion, and for MASI/BA N_w will increase, where

$$N_w = \frac{\int_0^f \Lambda(f')\,\mathrm{d}f'}{f} \tag{26}$$

A compilation of ACOMP values for M_w and $[\eta]_w$ at conversion points $f = 0.4$ and 0.8 are given in Tables 1 and 2. The general trend that MASI/MMA leads to decreasing mass (except 1B) and MASI/BA to increasing mass is seen. The root-mean-square radii of gyration, R_g, shown in Tables 1 and 2, are obtained from the viscosity data via the Flory relation, where $\Phi = 2.56 \times 10^{23}$

$$R_g \equiv \langle S^2 \rangle_V^{1/2} = \frac{1}{\sqrt{6}}\left(\frac{M[\eta]}{\Phi}\right)^{1/3} \tag{27}$$

GPC Data Reveal Time-Dependent Aggregation of Polymer. Figure 10 shows raw chromatograms for an initial aliquot containing MASI and MMA and for an aliquot of the reaction endproduct. The GPC measurements on these samples were made several days after the reaction. There is a small but visible LS peak at a very low elution volume, even below that of the main polymer LS peak from the aliquot taken after the reaction was over. This small peak is also present in the final aliquot. The reciprocal light scattering envelope of this small peak vs the angle-dependent scattering vector gives a large slope, indicating very large, aggregated structures. This corroborates the raw ACOMP data in Figure 1, where an unusually large amount of scattering was associated with the MASI monomer. This trend was found generally in ACOMP and pure monomer GPC data throughout the experiments and is linked to an aggregation process of MASI.

Similarly, copolymers containing MASI tended to aggregate in time. In Figure 10, the telltale existence of aggregates is seen by comparing the LS and RI raw GPC chromatograms for the initial and end products. The bimodal structure of the polymer peak region is inverted for LS and RI; i.e., the small population of massive aggregates at low elution volume gives a low RI signal and a large LS signal. Conversely, the high RI signal at the higher elution volume, corresponding to smaller structures, is accompanied by a much smaller LS signal.

Further, striking evidence of aggregation is seen in the inset to Figure 10, which shows Kc/I vs q^2 for homopolymeric MASI. The upward curvature is characteristic of dense, spheroidal scatterers. The curves shown are from different points in the elution spectrum. The lowest curves are for early elution, i.e., the highest masses, and the upper curves are for progressively higher elution volumes (lower masses).

Mass distributions from GPC (not shown) for all copolymers with MASI contain at least some aggregate component, seen as a small secondary peak or shoulder in the distributions. MMA and BA homopolymers are much smaller and have no second high-mass modes. Such aggregates are not present in the ACOMP results and presumably are due to a time-dependent aggregation and/or association occurring during the GPC elution.

Conclusions

ACOMP has allowed quantitative, model-independent determination of the copolymerization behavior of acrylate and methacrylate-based monomers in terms of kinetics, average composition, and composition drift, and the evolution of $[\eta]_w$ and M_w. The recently developed incorporation of a UV photodiode array detector into the ACOMP detector train, and the creation of a numerical approach to extracting instantaneous comonomer concentrations based on linear position of basis spectra over many wavelengths have made this possible.[28] Good resolution of comonomer concentrations at each instant of conversion, despite the low spectral contrast between MASI and MMA and MASI and BA, provides a striking example of how well this approach works even in this limit of low contrast. This type of resolution is not possible if only two wavelengths are used, such as in many previous ACOMP studies.

It was demonstrated how similar the copolymerization behavior of MASI and MMA are despite the very bulky and electron withdrawing side group of the methacrylate MASI. This contrasts to much more widely varying kinetics when a pair of acrylate and methacrylate comonomers is used, even when the latter do not have large side groups.

The results show how the large reactivity ratio differences in the MASI/MMA (methacrylate/methacrylate) and MASI/BA (methacrylate/acrylate) lead to narrower average composition distributions for the former and large downward composition drift for the latter.

Strikingly different trends in the evolution of M_w and reduced viscosity are observed between the MASI/MMA and MASI/BA series. Namely, the reactively similar MASI/MMA lead to M_w decreasing vs conversion, commonly seen in homopolymerization. The upward trend in M_w and $[\eta]_w$ for MASI/BA is linked to the large difference in reactivity ratios, the large difference in M_w for the homopolymers pMASI and pBA under similar polymerization conditions, as well as other possible effects such as non-QSSA conditions, and possible branching. During ACOMP measurements, there is no indication of aggregation, even with pure pMASI. However, all subsequent GPC data on endproducts, made days after each reaction, show that when MASI is involved, there are aggregates present.

This work sets the stage to more fully exploit the synthetic potential of MASI, particularly as it may be used in controlled radical, or "living" type reactions such as ATRP. It is expected that ACOMP will also be useful in following postpolymerization modifications such as hydrolysis and addition of specific functional groups. In addition, this work provides MASI reactivity ratios for two common monomers and should allow reasonable extrapolation to other methacrylate and acrylate monomers. These fundamental parameters are key to designing new synthetic macromolecules with tailored and controllable properties.

Acknowledgment. The Tulane authors acknowledge support from NSF CTS 0623531, NASA NCC3-946, and the Louisiana Board of Regents LINK program and ITRS RD-B-7. The University of Massachusetts authors acknowledge support from ARO (44266CHYIP). All the Tulane authors were displaced from New Orleans in August 2005 due to Hurricane Katrina. They would like to thank the members of the Polymer Science & Engineering Department at University of Massachusetts for the warm welcome extended to them in Katrina's aftermath. The current work was carried out at University of Massachusetts, and support from the NSF-funded MRSEC is also acknowledged. We further thank the following entities for generous help in terms of loans and equipment donations: Shimadzu Inc., Polymer Laboratories Inc., Arkema Inc., and Brookhaven Instruments Corp. The authors also acknowledge Tulane's permission to temporarily relocate some of the Tulane ACOMP instrumentation to University of Massachusetts.

References and Notes

(1) Coessens, V.; Pintauer, T.; Matyjaszewski, K. *Prog. Polym. Sci.* **2001**, *26*, 337.
(2) Liang, C.; Frechet, J. M. J. *Prog. Polym. Sci.* **2005**, *30*, 385.
(3) Stupp, S. I.; Pralle, M. U.; Tew, G. N.; Li, L. M.; Sayar, M.; Zubarev, E. R. *MRS Bull.* **2000**, *25*, 42.
(4) D'Agosto, F.; Charreyre, M. T.; Veron, L.; Llauro, M. F.; Pichot, C. *Macromol. Chem. Phys.* **2001**, *202*, 1689.
(5) Godwin, A.; Hartenstein, M.; Muller, A. H. E.; Brocchini, S. *Angew. Chem., Int. Ed.* **2001**, *40*, 594.
(6) Monge, S.; Haddleton, D. M. *Eur. Polym. J.* **2004**, *40*, 37.
(7) Relogio, P.; Charreyre, M. T.; Farinha, J. P. S.; Martinho, J. M. G.; Pichot, C. *Polymer* **2004**, *45*, 8639.
(8) Erout, M.-E.; Troesch, A.; Pichot, C.; Cros, P. *Bioconjugate Chem.* **1996**, *7*, 568.
(9) Savariar, E. N.; Thayumanavan, S. *J. Polym. Sci., Part A: Polym. Chem.* **2004**, *42*, 6340.
(10) Bergbreiter, D. E.; Case, B. L.; Liu, Y. S.; Caraway, J. W. *Macromolecules* **1998**, *31*, 6053.
(11) Shunmugam, R.; Tew, G. N. *J. Polym. Sci., Part A: Polym. Chem.* **2005**, *43*, 5831.
(12) Shunmugam, R.; Tew, G. N. *J. Am. Chem. Soc.* **2005**, *127*, 13567.
(13) Griffith, B. R.; Allen, B. L.; Rapraeger, A. C.; Kiessling, L. L. *J. Am. Chem. Soc.* **2004**, *126*, 1608.
(14) Allen, M. J.; Raines, R. T.; Kiessling, L. L. *J. Am. Chem. Soc.* **2006**, *128*, 6534
(15) Vosloo, J. J.; Tonge, M. P.; Fellows, C. M.; D'Agosto, F.; Sanderson, R. D.; Gilbert, R. G. *Macromolecules* **2004**, *37*, 2371.
(16) D'Agosto, F.; Charreyre, M. T.; Pichot, C. *Macromol. Biosci.* **2001**, *1*, 322.
(17) Hermanson, G. *Bioconjugate Techniques*; Academic Press: New York, 1996; p 139.
(18) Tew, G. N.; Aamer, K.; Shunmugam, R. *Polymer* **2005**, *46*, 8440.
(19) Florenzano, F. H.; Strelitzki, R.; Reed, W. F. *Macromolecules* **1998**, *31*, 7226.
(20) Giz, A.; Catalgil-Giz, H.; Alb, A. M.; Brousseau, J. L.; Reed, W. F. *Macromolecules* **2001**, *34*, 1180.
(21) Chauvin, F.; Alb, A. M.; Bertin, D.; Tordo, P.; Reed, W. F. *Macromol. Chem. Phys.* **2000**, *203*, 2029.
(22) Mignard, E.; Lutz, J.-F.; Matyjaszewski, K.; Guerret, O.; Reed, W. F. *Macromolecules* **2005**, *38*, 9556.
(23) Farinato, R. S.; Calbick, J.; Sorci, G. A.; Florenzano, F. H.; Reed, W. F. *Macromolecules* **2005**, *38*, 1148.
(24) Catalgil-Giz, H.; Giz, A.; Alb, A. M.; Oncul A. K.; Reed, W. F. *Macromolecules* **2002**, *35*, 6557.
(25) Grassl B.; Alb A. M.; Reed, W. F. *Makromol. Chem. Phys.* **2001**, *12*, 2518.
(26) Alb, A. M.; Farinato, R.; Calbeck, J.; Reed, W. F. *Langmuir* **2006**, *22*, 831.
(27) Reed, W. F. *Macromolecules* **2000**, *33*, 7165.
(28) Alb, A. M.; Enohnyaket, P.; Drenski, M. F.; Head, A.; Reed, A. W.; Reed, W. F. *Macromolecules* **2006**, *39*, 5705.
(29) Chauvin, F.; Alb, A.; Bertin, D.; Tordo, P.; Reed, W. F. *Macromol. Chem. Phys.* **2002**, *203*, 2029.
(30) Mignard, E.; Leblanc, T.; Bertin, D.; Guerret, O.; Reed, W. F. *Macromolecules* **2004**, *37*, 966.
(31) Norwood, D. P.; Reed, W. F. *Int. J. Polym. Anal. Charact.* **1997**, *4*, 99.
(32) Kelen, T.; Tudos, F. *J. Macromol. Sci.* **1975**, *A9*, 1.
(33) Ziegler, M. J.; Matyjaszewski, K. *Macromolecules* **2001**, *34*, 415.
(34) Rodriguez, F. *Principles of Polymer Systems*, 3rd ed.; Hemisphere Publishing. Corp.: Bristol, PA, 1989.
(35) Odian, G. *Principles of Polymerization*, 3rd ed.; John Wiley & Sons: New York, 1991.
(36) Stockmayer, W. H.; Moore, L. D.; Fixman, M.; Epstein, B. N. *J. Polym. Sci.* **1955**, *16*, 517.
(37) Bushuk, W.; Benoit, H. *Can. J. Chem.* **1958**, *36*, 1616.
(38) Scott, G.E.; Senogles, E. *J. Macromol. Sci. Chem.* **1970**, *A4*, 1105.
(39) Madruga, E. L.; Fernandez-Garcia, M. *Macromol. Chem. Phys.* **1996**, *197*, 3743.
(40) McKenna, T. F.; Villanueva, A.; Santos, A. M. *J. Polym. Sci., Part A: Polym Chem.* **1999**, *37*, 571.
(41) Kaszas, G.; Foldes-Berezsnich, T.; Tudos, F. *Eur. Polym. J.* **1983**, *19*, 469.
(42) Fernandez-Garcia, M.; Fernandez-Sanz, M.; Madruga, E. L. *Macromol. Chem. Phys.* **2000**, *201*, 1840.
(43) Scott, G. E.; Senogles, E. *J. Macromol. Sci. Chem.* **1974**, *A8*, 753.
(44) Nikitin, A. N.; Hutchinson, R. A. *Macromolecules* **2005**, *38*, 1581.
(45) Nikitin, A. N.; Hutchinson, R. A. *Macromol. Theory Simul.* **2006**, *15*, 128.
(46) Ydens, I.; Degée, P.; Haddleton, D. M.; Dubois, P. *Eur. Polym. J.* **2005**, *41*, 2255.
(47) Jone Selvamalar, C. S.; Penlidis, A.; Nanjundan, S. *J. Macromol. Sci., Part A* **2003**, *40*, 1019.
(48) Pang, X. A.; Sun, H. M.; Shen, Q. *Polymer* **2004**, *45*, 4029.
(49) Erol, I.; Soykan, C. *J. Macromol. Sci.* **2002**, *A39*, 953.
(50) Han, Z.; Lu, C.; Wu, Y.; Wu, P.; Zhu, Q. Gaofenzi Cailiao Kexue Yu Gongcheng **1997**, *13*, 28.
(51) Camail, M.; Essaoudi, H.; Margaillan, A.; Vernet, J. L. *Eur. Polym. J.* **1995**, *31*, 1119.
(52) Yong, T. Y.; van Ekenstein, G.; Alberda, O. R. *Eur. Polym. J.* **1994**, *30*, 1363.
(53) Jayakumar, R.; Balaji, R.; Nanjundan, S. *Eur. Polym. J.* **2000**, *36*, 1659.
(54) Coskun, M.; Ilter, Z. *J. Polym. Sci., Part A: Polym. Chem.* **2002**, *40*, 1184.

MA0616864